Copyright © 1983 American Telephone and Telegraph Company
THE BELL SYSTEM TECHNICAL JOURNAL
Vol. 62, No. 2, February 1983
Printed in U.S.A.

High-Frequency Impedance of Proton-Bombarded Injection Lasers

By B. W. HAKKI, W. R. HOLBROOK, and C. A. GAW

(Manuscript received August 11, 1982)

Experimental and theoretical results are given of an investigation of the capacitance behavior with frequency of GaAs injection lasers. It is shown that, for shallow-bombarded stripe geometry lasers, the zero-bias capacitance decreases rapidly beyond a certain frequency. This is interpreted in terms of confinement of the low-level radio frequency current under the stripe at high frequencies. Comparison of the experimental results with the analytically derived expressions provides a measure of the material resistivity adjoining the active region. This inferred material resistivity is shown to be in good agreement with results obtained by more direct measurements. Finally, the general conclusions are also applicable to other optoelectronic devices operating at high frequency, such as light-emitting diodes.

I. INTRODUCTION

Injection lasers are inherently suited for high-frequency (>50 MHz) applications.[1,2] In the Bell System, the commonly used GaAs double-heterostructure (DH) stripe geometry laser is obtained by either shallow- or deep-proton bombardment.[3,4] For deep bombardment, the active stripe is well defined electrically by the high-resistivity material that confines it. In the case of shallow bombardment, as well as oxide stripe geometry lasers, current can flow laterally, beyond the stripe, through the conductive cladding layer.[5–8]

Previously, the impedances of several laser geometries were measured at high frequencies, and the results interpreted in terms of phenomenological equivalent circuits.[9–13] In this paper, we will restrict the analysis and measurements to zero-biased shallow-bombarded laser diodes, for simplicity. We will show that, for shallow-bombarded stripe geometry lasers, the low-level (radio frequency) RF current at

high frequencies is confined under the stripe. The interpretation of measurements in terms of the fundamentally derived analytical expressions provides a useful measure of relevant material properties. Finally, although the main emphasis is on stripe geometry lasers, the analysis is applicable to other optoelectronic devices. Thus, the approach can be applied to predict the small-signal, unbiased impedance of light-emitting diodes (LEDs) and photodetectors operating at high frequencies.

II. EXPERIMENT

The injection laser is a standard GaAs DH grown by either liquid phase epitaxy (LPE) or molecular beam epitaxy (MBE) technology.[14,15] It consists of 2-μm-thick N-$Ga_{1-x}Al_xAs$ cladding, 0.1- to 0.2-μm $Ga_{1-y}Al_yAs$ active, 1.5-μm P-$Ga_{1-x}Al_xAs$ cladding, and, finally, 0.5-μm p-GaAs contact layer. Shallow-proton bombardment is used to define stripe widths of either 5- or 10-μm dimension. For these measurements, it is essential to obtain an accurate measure of the stripe width, $2S$, and the distance of separation, d_A, between the active region and the semi-insulating damaged region. This is done by etching the mirror facets in a dilute A/B solution.[16] An example of such an etched mirror obtained by a scanning electron microscope (SEM) is shown in Fig. 1a. Figure 1b is a schematic of the various layers. The distance, d_A, is between the unetched region and the active layer. It is assumed that the etch stops abruptly where the conductivity changes from p-type to semi-insulating. (In general, this is a fair assumption, although it may not be accurate to better than 0.1 μm.)

Every diode is subjected to dc current-voltage and ac impedance tests. The dc measurement determines rectification properties, and current-voltage dependence over the range between 10^{-12} to 10^{-2} amperes. The ac impedance test used RF signal levels, at or below 50 mV, performed on unbiased diodes. At those RF signal levels, the diode conduction current is less than 10^{-11} amperes. The laser impedance is measured at zero bias over a frequency range extending from 10^4 to 5×10^7 Hz. Over this frequency range the capacitive current is typically larger than 10^{-6} amperes. Hence, in the present impedance measurements, the junction capacitive current is well over 10^5 times greater than the diode conduction current. Therefore, for our purposes, the junction can be assumed to be a capacitance with negligible rectified current flow.

Usually, two capacitance bridges are used at different frequency ranges, with an overlap in frequency to ensure accuracy. These impedance bridges measure the equivalent parallel capacitance and conductance of the diode. As an example, Fig. 2 shows the results of two such measurements and two experimental values when results were

(a)

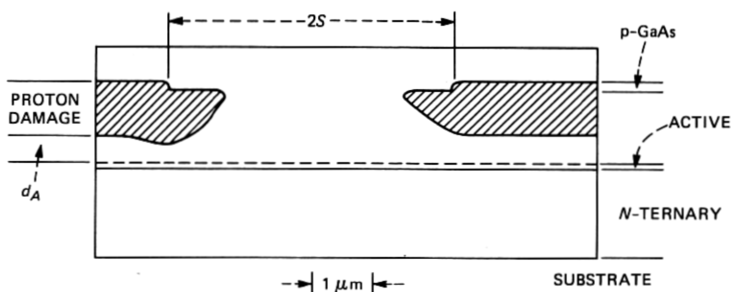

(b)

Fig. 1—Mirror of shallow-bombarded stripe geometry DH GaAs layer after etching in dilute A/B etch. (a) Photomicrograph of the etched mirror as obtained by an SEM. In this case, the p-active layer has also been etched. (b) Layer schematic of the same mirror.

obtained on two different instruments. In Fig. 2a, the zero bias capacitance of diode A14 (grown by LPE) is constant as a function of frequency up to 1 MHz. Above 1 MHz, the equivalent parallel circuit capacitance decreases rapidly with an increase in frequency. The same general behavior is observed on another diode from a different slice. The results of diode B22 (grown by MBE) are shown in Fig. 2b. The zero bias capacitance decreases abruptly for frequencies in excess of 10^5 Hz. We also find that, for both diodes, the equivalent parallel circuit conductances G increase with frequency f according to the relation $G \propto f^n$, where n is between 1.25 and 1.5. However, accurate measurements of conductance are more difficult to obtain than those of capacitance.

The results of Fig. 2 show the abrupt drop in capacitance at frequencies that may differ by as much as an order of magnitude. Furthermore, some devices exhibit a more gradual reduction in the capacitance-frequency behavior.[17] Figure 3 shows an example of such a soft roll-off in the measured capacitance. The solid curve is the modified analysis, which accounts for asymmetry and metallization capacitance. The dashed theoretical curve is for the ideal symmetric

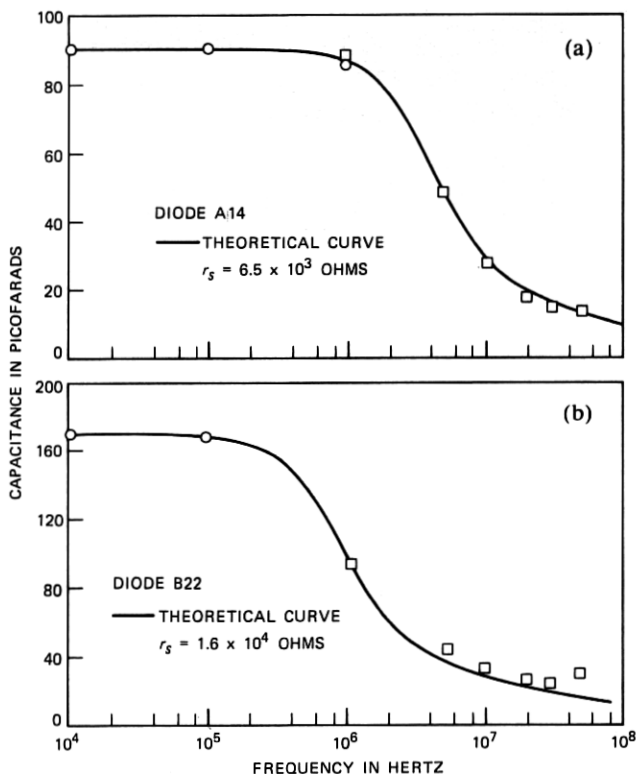

Fig. 2—Capacitance dependence on frequency for (a) diode A14 and (b) diode B22. The solid curves are obtained from analytical expressions. In (a) and (b), d_A is 0.6 and 0.21 μm, respectively.

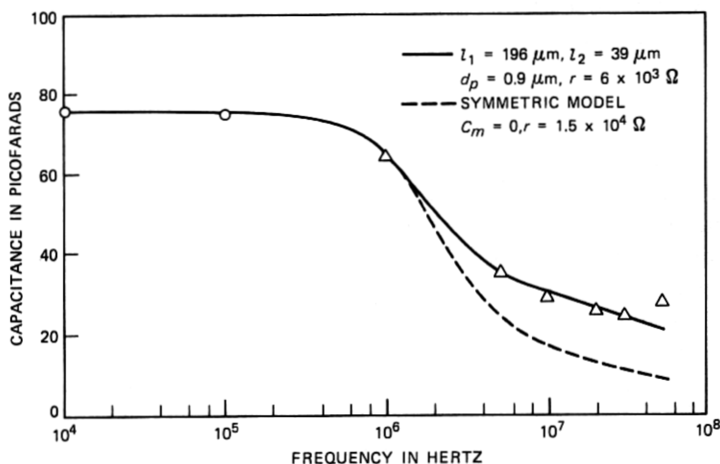

Fig. 3—Capacitance dependence on frequency for a severely eccentric stripe geometry device.

model. The distance between the stripe and the two edges, l_1 and l_2, respectively, as well as the thickness of the damaged region, d_p, are obtained from SEM measurements. Here, the high-frequency capacitance does not decrease as rapidly as that for the cases shown in Fig. 2.

III. ANALYSIS

3.1 The ideal symmetric case

Consider first the simple and ideal case of a stripe centered within the chip. In addition, assume that the proton-damaged region is sufficiently thick (greater than 2.5 micrometers), so that the only relevant capacitance is the junction capacitance. The RF current flows through the diode as shown schematically in Fig. 4a. There is a direct stripe capacitance, C_s, defined by the width $2S$ and length L of the stripe. The RF current flows through the adjoining cladding layer, which, together with the junction, forms a transmission line. This transmission line is shown schematically in Fig. 4b. It consists of a distributed resistance, r, and a distributed capacitance, c. The analysis of such a transmission line is straightforward. The cladding sheet resistance, r_s, is equal to ρ/d_A, where ρ is the average material resistivity. The capacitance per unit area is c_a given by C_0/A, where C_0 is the low-frequency total diode capacitance and A is the total diode area. In the equivalent distributed parameter circuit shown in Fig. 4b, the resistance per unit length r is equal to r_s/L. Similarly, the capacitance per unit length c is equal to c_aL. At any point x, the current and voltage are given, respectively, by

$$i(x, t) = I(x)e^{j\omega t} \tag{1}$$

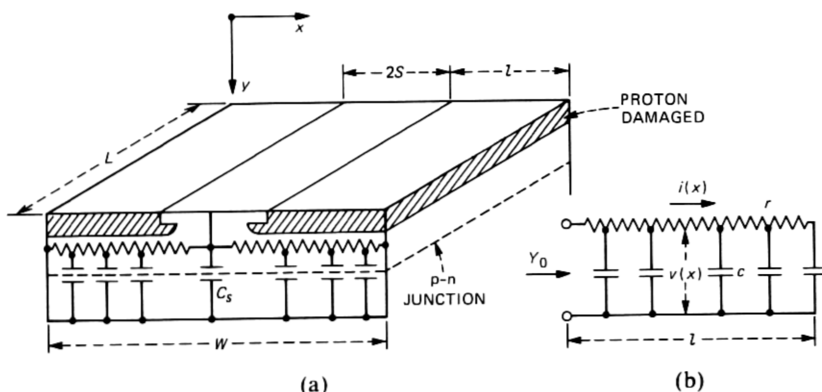

Fig. 4—Schematic of shallow-proton-bombarded, ideally symmetric, stripe geometry laser and equivalent circuit. (a) The various layers and the electrical elements. (b) The distributed parameter transmission line underneath the proton-bombarded region.

and

$$v(x, t) = V(x)e^{j\omega t}. \tag{2}$$

The spatial parts of the current and voltage are related by the equations

$$\frac{dV}{dx} = -rI \tag{3}$$

and

$$\frac{dI}{dx} = -j\omega cV. \tag{4}$$

These are almost standard transmission line equations that have to be solved with the boundary condition $I(\ell) = 0$, where $\ell = (W/2)\text{-}S$. This open-circuit boundary condition is appropriate when surface leakage is negligible. The input admittance, Y_0, is given by

$$Y_0 = G_0 + jB_0, \tag{5}$$

where

$$G_0 = \frac{\phi}{2r\ell}\frac{\sinh\phi - \sin\phi}{\cosh\phi + \cos\phi}, \tag{6a}$$

$$B_0 = \frac{\phi}{2r\ell}\frac{\sinh\phi + \sin\phi}{\cosh\phi + \cos\phi} \tag{6b}$$

and

$$\phi = \ell\sqrt{2\omega rc}. \tag{6c}$$

From the susceptance given in (6b), an equivalent distributed parallel capacitance, C_d, is obtained in the form

$$\frac{C_d}{C_0'} = \frac{1}{\phi}\frac{\sinh\phi + \sin\phi}{\cosh\phi + \cos\phi}, \tag{7}$$

where $C_0' = c_a\ell L$ is the low-frequency capacitance of the junction whose area is ℓL. A plot of C_d/C_0' is shown in Fig. 5 as a function of ϕ. It is seen that the equivalent distributed parallel capacitor value remains equal to the low-frequency value as long as $\phi < 1$. However, for $\phi > 1$, the capacitance decreases at the rate of $1/\phi$. This decrease at high frequency is due to the fact that as the frequency increases, a relatively larger fraction of the reactive current is shunted by the distributed capacitance at small distances. At sufficiently high frequencies most of the current is bypassed at small distance by the capacitance.

The choice of a parallel circuit, unfortunately, does not provide a straightforward connection between conductance and the material

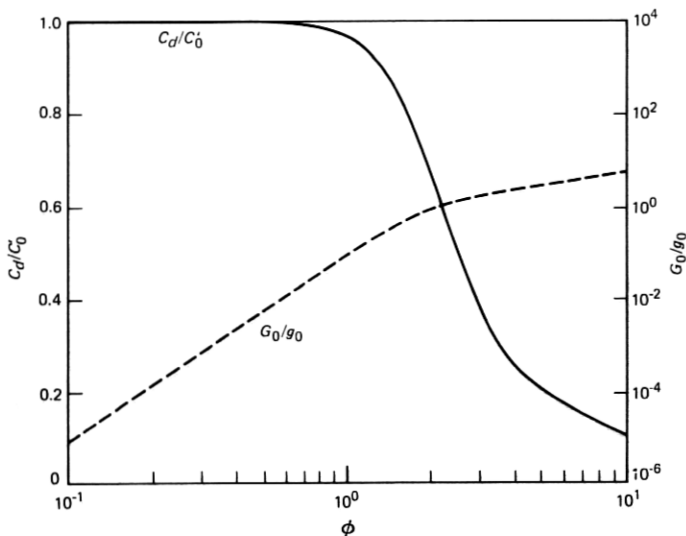

Fig. 5—Equivalent parallel circuit capacitance and conductance for the distributed transmission line of Fig. 4b. The variation is in terms of the normalized parameter, ϕ, defined in the text.

resistivity. Nevertheless, let $g_0 = Ld_A/\rho\ell$, which is the dc conductance between $x = 0$ and ℓ. Then, G_0/g_0 is plotted as a function of ϕ in Fig. 5. It is seen that the normalized conductance increases as ϕ^4. Since ϕ varies as $f^{1/2}$, it follows that the conductance increases as f^2, which is somewhat faster than the experimentally observed variation.

The above results can be applied to the ideally symmetric stripe geometry configuration of Fig. 4a. The total equivalent parallel capacitor of the diode C_p, comprising the direct stripe and distributed capacitances, respectively, is given by

$$C_p = C_0 \left[\frac{A_s}{A} + \left(1 - \frac{A_s}{A}\right) \frac{\sinh \phi + \sin \phi}{\phi(\cosh \phi + \cos \phi)} \right], \tag{8}$$

where $A_s = 2SL$ is the area of the stripe, C_0 is the total capacitance of the diode at low frequency, and the rest of the parameters are as defined previously.

Figure 2a shows a plot of eq. (8), with a sheet resistance chosen at a value of 6.5×10^3 ohms. The stripe width is 5 μm, the diode width is 250 μm, and the length is 380 μm. The stripe width is obtained by etching the mirror, as in Fig. 1. The only adjustable parameter in the curve of Fig. 2a is the sheet resistance. A similar theoretical curve is plotted in Fig. 2b for diode B22. Here, the stripe width is 10 μm, and the sheet resistance is 1.6×10^4 ohms. It is seen that the capacitance in Fig. 2b starts to decrease at a lower frequency because of the higher

sheet resistance. The high sheet resistance in diode B22 is due to the smaller distance of separation between the damaged region and the active layer.

3.2 Asymmetric stripe with metallization capacitance

Two deviations from the earlier symmetric model are observed in some devices. First, the stripe can be eccentric. Second, the proton-damaged layer can be as thin as 0.5 micrometers. These two factors cause the high-frequency behavior to deviate from the ideal model. This has been noted in independent measurements by C. W. Thompson et al.[17]

The metallization can contribute a significant additional capacitance if the metallization is separated from the conducting semiconductor by a thin insulating layer. Such a condition can exist in oxide stripe geometry lasers as well as in some proton-bombarded lasers. However, this capacitance has unique characteristics, since it is not operative at low frequencies, where the electrodes are virtually connected. But at high frequencies, charge storage between the metal and the semiconductor can take place. A schematic of the various layers is shown in Fig. 6a. The proton-damaged layer thickness is d_p. This semi-insulating layer can, at high frequencies, contribute a metallization capacitance C_m given approximately for GaAs by

$$C_m \approx 10/d_p \qquad pF, \tag{9}$$

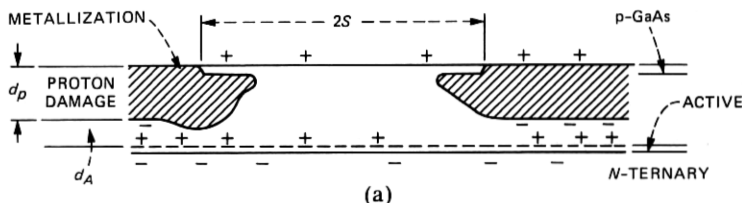

(a)

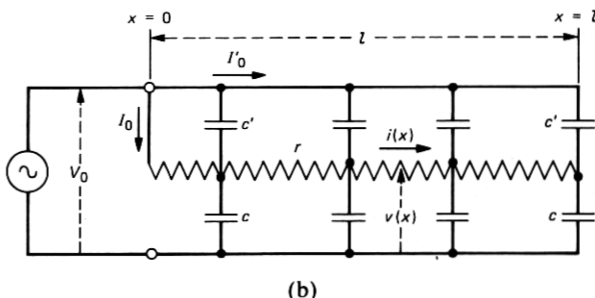

(b)

Fig. 6—Schematic of stripe geometry with thin damaged layer. (a) Charge buildup. (b) Equivalent transmission line circuit. The metallization capacitance results from charge storage across the proton-bombarded region.

where d_p is measured in micrometers, and the chip is 250×380 μm, which is typical for our diodes. For oxide-defined stripe geometry lasers, the metallization capacitance is associated with the oxide layer itself.

The metallization capacitance is not effective at low frequencies. This is obvious from Fig. 6a, where conduction through the stripe region bypasses the charge across the damaged region. The equivalent transmission line circuit is shown schematically in Fig. 6b.[18] The circuit parameters are as defined previously, and solution of the transmission line equations follows the usual procedures. The total current branches into two components, I_0 and I_0', respectively. The two admittances are given by

$$G_0' = \frac{\omega c c' \ell}{(c + c')} \left[\frac{\sinh \phi - \sin \phi}{\phi(\cosh \phi + \cos \phi)} \right] \tag{10a}$$

$$G_0 = \omega c \ell \left[\frac{\sinh \phi - \sin \phi}{\phi(\cosh \phi + \cos \phi)} \right] \tag{10b}$$

$$B_0' = \frac{\omega c c' \ell}{(c + c')} \left[1 - \frac{\sinh \phi + \sin \phi}{\phi(\cosh \phi + \cos \phi)} \right] \tag{10c}$$

$$B_0 = \omega c \ell \frac{(\sinh \phi + \sin \phi)}{\phi(\cosh \phi + \cos \phi)}, \tag{10d}$$

where

$$\phi = \ell\sqrt{2\omega r(c + c')},$$
$$c' = C_m/W, \tag{10e}$$

and W is the total width of the chip.

Since the two admittances are in parallel, the equivalent parallel circuit capacitance is

$$C = \frac{C_0}{C_0 + C_m} \left[C_0 \frac{\sinh \phi + \sin \phi}{\phi(\cosh \phi + \cos \phi)} + C_m \right], \tag{11}$$

where C_0 is the low-frequency junction capacitance, and C_m is the metallization capacitance, as given in (9). It is clear from (11) that at low frequency, the ϕ function goes to one, and the capacitance becomes equal to the low-frequency junction capacitance. On the other hand, at high frequency, the ϕ function goes to zero, and the capacitance becomes equal to the metallization and the junction capacitances in series.

When the stripe is located off-center, the capacitance can be calculated in a straightforward manner. The total chip capacitance becomes

$$C_T = C_0 \left\{ \frac{A_s}{A} + \left(\frac{1 - A_s/A}{C_0 + C_m} \right) \left[\frac{C_0}{(\ell_1 + \ell_2)} (\ell_1 F_1 + \ell_2 F_2) + C_m \right] \right\}, \tag{12}$$

where

$$F_i = \frac{\sinh \phi_i + \sin \phi_i}{\phi_i(\cosh \phi_i + \cos \phi_i)}, \tag{13}$$

$$\phi_i = \ell_i\sqrt{2\omega r(c + c')}, \tag{14}$$

$$\ell_1 + \ell_2 + 2S = W, \tag{15}$$

ℓ_1 and ℓ_2 are the lengths of the two distributed line sections, respectively, $2S$ is the stripe width, A_s is the total area of the stripe, and A is the area of the diode.

An example of a case of extreme asymmetry is shown in Fig. 3. Measurement of eccentricity indicates that the stripe is displaced by $\approx$70 μm from its center position. The measured thickness of the proton-damaged region is 0.9 μm, which results in a metallization capacitance of 11 pF. When the expression for the asymmetric case, as given in (12), is applied to the results of Fig. 3, the agreement between theory and experiment is adequate for a sheet resistance of $6 \times 10^3\,\Omega$. On the other hand, the symmetric model, shown as a dashed curve in Fig. 3, cannot fit the data over the extended frequency range. In addition, the symmetric model overestimates the sheet resistance.

3.3 *Material resistivity*

Having obtained a value of sheet resistance and layer thickness, d_A, the material resistivity can be derived. However, care should be exercised in accounting for proton damage spread into the conductive layer.

If $y = 0$ is the point at the edge of the damaged region where the local carrier concentration is (mathematically) zero, then for $y > 0$, the carrier concentration does not recover abruptly as a step function. Instead, the carrier concentration actually recovers as an error function of distance.[19] For our purposes, this recovery can be represented approximately by the relation

$$p(y) = p_0(1 - e^{-y/y_0}), \tag{16}$$

where p_0 is the background-free hole concentration, and y_0 determines the rate at which carrier removal decreases with distance.

For current flow parallel to the junction plane, the average resistivity ρ over a thickness d_A is

$$\rho = \rho_0 \Big/ \left\{1 - \frac{y_0}{d_A}\left[1 - \exp(-\,d_A/y_0)\right]\right\}, \tag{17}$$

where ρ_0 is the resistivity of the undamaged material. From published data of proton-bombarded GaAs, it would seem that the value of y_0 is $0.13 \mp .03$ μm.[19–21]

The above equations can now be applied to the results of Fig. 2. For diode A14 we obtain $\rho = 0.39\ \Omega$-cm; and $\rho_0 = 0.3\ \Omega$-cm. For diode B22, we obtain $\rho = 0.34\ \Omega$-cm, and $\rho_0 = 0.17\ \Omega$-cm. Several diodes from these slices were measured. The results were averaged and given in Table I. The average resistivity in the cladding, adjacent to the active region, in slice A is $0.28 \mp 0.09\ \Omega$-cm. Direct measurement of resistivity in this material by J. L. Zilko gives a value of $0.21\ \Omega$-cm.[22] Hence, to within statistical diode-to-diode variation, the agreement is adequate. The resistivity of the cladding in slice B, given in Table I, is $0.18 \mp 0.02\ \Omega$-cm. These resistivities can also be used to estimate the free-hole concentration. For the typical 40-percent aluminum in the ternary, the hole mobility should be about 100 cm^2/Vs.[23,24] The deduced-hole concentrations for slices A and B are listed in Table I. To check these deduced values with direct-hole concentration measurements, a third slice C was evaluated. The hole concentration, in slice C in the cladding, as deduced from the capacitance-frequency measurement, was $(2.1 \mp 0.6) \times 10^{17}\ cm^{-3}$. On the other hand, hole-concentration measurements on this slice, by the automatic feedback method,[21] gave values of $(1.9 \mp 0.4) \times 10^{17}\ cm^{-3}$.[25] Hence, again the capacitance-frequency method gave values consistent with those obtained by other methods.

Stripe geometry lasers with deep-proton bombardment were also evaluated. In these devices the proton damage extends beyond the active region. Here, as opposed to the results for shallow bombardment, the capacitance remains small and nearly invariant with frequency. This again lends support to the model of RF current confinement in shallow-bombarded stripe geometry lasers.

IV. CONCLUSION

Experiments conducted on shallow proton-bombarded stripe geometry lasers show that the capacitance decreases abruptly above a certain frequency. These results are interpreted in terms of a distributed parameter transmission line model. It is shown that the frequency beyond which the capacitance decreases depends on: the sheet resistance of the material above the active region, capacitance per unit area,

Table I—Material evaluation obtained from capacitance frequency measurements

	Slice Average				
Slice	r_s ohms	ρ ohms-cm	d_A μm	ρ_0 ohm-cm	p_0 cm^{-3}
A	$(6 \mp 2) \times 10^3$	0.37 ∓ 0.12	0.6	0.28 ∓ 0.09	$(2.5 \mp 0.9) \times 10^{17}$
B	$(1.5 \mp 0.1) \times 10^4$	0.36 ∓ 0.03	0.22 ∓ 0.02	0.18 ∓ 0.02	$(3.4 \mp 0.4) \times 10^{17}$

and the dimension of the diode. These analytical expressions, when applied to experimental results, allow one to obtain an estimate of the material resistivity adjoining the active region. The deduced values of resistivity and doping concentration are in good agreement with the values obtained by other methods.

Although the analytical results are applied to laser structures, they are also applicable to other optoelectronic devices. For instance, the same general conclusions can also be drawn about the small signal impedance of LEDs operating at high frequency. For configurations other than the simple stripe geometry, the spatial distribution of RF current obviously changes. However, the qualitative results are the same.

V. ACKNOWLEDGMENT

The authors are indebted to A. E. Bakanowski, H. E. Elder, E. I. Gordon, and C. W. Thompson, Jr., for useful discussions, and to A. Y. Cho and M. C. Tamargo for providing the laser material. The authors are also grateful to J. L. Zilko for providing independent resistivity measurements, and to C. G. Bergey and E. W. Bonato for detailed measurements.

REFERENCES

1. S. E. Miller, E. A. J. Marcatili, and Tingye Li, "Research Toward Optical-Fiber Transmission Systems—Part I," Proc. IEEE, *61* (December 1973), pp. 1703–26.
2. S. E. Miller, Tingye Li, and E. A. J. Marcatili, "Research Toward Optical-Fiber Transmission Systems—Part II," Proc. IEEE, *61* (December 1973), pp. 1726–51.
3. J. C. Dyment, L. A. D'Asaro, J. C. North, B. I. Miller, and J. E. Ripper, "Proton-Bombardment Formation of Stripe Geometry Heterostructure Lasers for 300°K CW Operation," Proc. IEEE, *60* (June 1972), pp. 726–28.
4. B. W. Hakki, "Carrier and Gain Spatial Profiles in GaAs Stripe Geometry Lasers," J. Appl. Phys., *44* (November 1973), pp. 5021–28.
5. B. W. Hakki, "GaAs Double Heterostructure Lasing Behavior Along the Junction Plane," J. Appl. Phys., *46* (January 1975), pp. 292–302.
6. W. B. Joyce, "Current Crowding and Carrier Confinement in Double Heterostructure Lasers," J. Appl. Phys., *51* (May 1980), pp. 2394–2401.
7. H. Yonezu, I. Sakuma, K. Kobayashi, T. Kamejima, M. Unno, and Y. Nannichi, "A GaAs/$Al_xGa_{1-x}As$ Double Heterostructure Planar Laser," Jpn. J. Appl. Phys., *12* (October 1973), pp. 1585–92.
8. W. P. Dumke, "Current Thresholds in Stripe-Contact Injection Lasers," Solid State Electron., *16* (November 1973), pp. 1279–98.
9. F. K. Reinhart, "Reverse-Biased Gallium Phosphide Diodes as High-Frequency Light Modulators," J. Appl. Phys., *39* (June 1968), pp. 3426–34.
10. K. Aiki, M. Nakamura, T. Kuroda, K. Umeda, R. Ito, N. Chinone, and M. Maeda, "Transverse Mode Stabilized (AlGa)As Injection Lasers with Channeled-Substrate-Planar Structure," IEEE J. Quantum Electron., *14* (February 1978), pp. 89–94.
11. K. Furuya, Y. Suematsu, and T. Hong, "Reduction of Resonance-Like Peak in Direct Modulation Due to Carrier Diffusion in Injection Laser," Appl. Optics, *17* (June 1978), pp. 1949–52.
12. H. Kuwahara, Y. Daido, and H. Furuta, "Measurements of Impedance of DH Semiconductor Lasers," Proc. IEEE, *65* (September 1977), pp. 1412–13.
13. J. M. Dumant, Y. Guillausseau, and M. Monerie, "Small Signal Modulation of DH Laser Diodes: Effect of the Junction Capacitance," Optics Commun., *33* (February 1980), pp. 188–92.

14. L. R. Dawson, "Near-Equilibrium LPE Growth of GaAs-$Ga_{1-x}Al_xAs$ Double Heterostructures," J. Cryst. Growth, *27* (December 1974), pp. 86–96.
15. A. Y. Cho and H. C. Casey, Jr., "GaAs-$Al_xGa_{1-x}As$ Double-Heterostructure Lasers Prepared by Molecular Beam Epitaxy," Appl. Phys. Letters, *25* (September 1974), pp. 288–90.
16. J. C. Campbell, S. M. Abott, and A. G. Dentai, "A Comparison of 'Normal' Lasers and Lasers Exhibiting Light Jumps," J. Appl. Phys., *51* (August 1980), pp. 4010–13.
17. C. W. Thompson, Jr., H. E. Elder, and A. E. Bakanowski, private communication.
18. A. E. Bakanowski, private communication.
19. H. Matsumura, and K. Stephens, "Electrical Measurement of the Lateral Spread of the Proton Isolation Layer in GaAs," J. Appl. Phys., *48* (July 1977), pp. 2779–83.
20. B. R. Pruniaux, J. C. North, and G. L. Miller, "Compensation of n-Type GaAs by Proton Bombardment," Proc. 2nd Int. Conf. on Ion Implantation, edited by I. Ruge and J. Graul, New York: Springer-Verlag, 1971, pp. 212–27.
21. G. L. Miller, "A Feedback Method for Investigating Carrier Distributions in Semiconductors," IEEE Trans. Electron. Dev., *ED-19* (October 1972), pp. 1103–8.
22. J. L. Zilko, and P. J. Anthony, "Conductivity Profiling of GaAs/GaAlAs Multilayer Structures," J. Electrochem. Soc., *128* (April 1981), pp. 871–74.
23. S. Zukotynski, S. Sumski, M. B. Panish, and H. C. Casey, Jr., "Electrical Properties of Ge-Doped p-type $Al_xGa_{1-x}As$," J. Appl. Phys., *50* (September 1979), pp. 5795–99.
24. A. J. SpringThorpe, F. D. King, and A. Becke, "Te and Ge-Doping Studies in $Ga_{1-x}Al_xAs$," J. Electron. Materials, *4* (February 1975), pp. 101–18.
25. B. W. Hakki, "p-GaAs/P-$Ga_{1-x}Al_xAs$ Isotype Heterojunctions in Doubleheterostructure Laser Material," J. Appl. Phys., *52* (October 1981), pp. 6054–58.